# Modeling and Characterization of a ReBCO HTS Degaussing Demonstrator

Hanse, I.; Wikkerink, D. P.; Keijzer, R.; Dhalle, M.; ten Kate, H.H.J.; ter Brake, H.J.M.

**Citation (APA)**
Hanse, I., Wikkerink, D. P., Keijzer, R., Dhalle, M., ten Kate, H. H. J., & ter Brake, H. J. M. (2022). Modeling and Characterization of a ReBCO HTS Degaussing Demonstrator. *IEEE Transactions on Applied Superconductivity*, *32*(6), 1-5. Article 4901705. https://doi.org/10.1109/TASC.2022.3180967

**Important note**
To cite this publication, please use the final published version (if applicable).
Please check the document version above.

# Modeling and Characterization of a *Re*BCO HTS Degaussing Demonstrator

I. Hanse , D. P. Wikkerink, R. Keijzer, M. Dhallé, H. H. J. ten Kate , and H. J. M. ter Brake

*Abstract*—The magnetic modelling and experimental validation of a superconducting degaussing system for maritime vessels is discussed. Degaussing coils compensate for the distortion in the earths' magnetic field by the magnetized steel hull of a ship, thus rendering it 'invisible' for magnetic field sensors. Whereas typical power requirements with copper coils are of the order of 100 kW, a *Re*BCO HTS degaussing system in principle allows to reduce this by an order of magnitude. In order to validate such efficiency estimates and to demonstrate the required hardware, a table-top test setup was realized with magnetic ship steel. The vessel-imitating cylindrical demonstrator is equipped with six degaussing coils, grouped in three sets that act in two different directions, with each set consisting of one copper and one *Re*BCO coil, the latter one equipped with a sub-cooled forced-flow liquid nitrogen system. Static magnetic field measurements are reported and compared to both analytical and numeric finite element models. The results illustrate how even relatively simple analytical models can be used as a powerful tool to extrapolate design parameters and thus to predict the power requirements of large-scale degaussing systems.

*Index Terms*—2G HTS conductors, finite element methods, HTS Cables, HTS coils, modeling.

## I. INTRODUCTION

**D**EGAUSSING systems are used to compensate the distortion of earths' magnetic field caused by the magnetized steel hull of a ship. These systems have been used since the beginning of world war II to reduce the magnetic signature of ships. The magnetic signature of naval vessels can be caused by different reasons including the magnetic steel in the hull of the ship, roll-induced eddy currents, corrosion-related sources and stray fields [1]–[3]. The need for degaussing systems was introduced because of the use of Magnetic Anomaly Detectors (MADs) and underwater mines [4]. MADs are usually airborne detectors that can detect the presence of a ship while underwater mines are mines that are set to go off as soon as a certain magnetic signature of disturbance is detected.

A lot of research was performed to improve the quality of degaussing systems by creating models to accurately determine magnetic signatures [3], [5], [6] and by improving the accuracy of the degaussing systems themselves [4], [7].

One major disadvantages of degaussing systems is the high power consumption of up to several 100 kW [8]. Many coils are needed in three different directions, with currents of up to 1500 A [4]. To reduce the energy consumption of degaussing systems, superconductivity can play a role. Kephart and Fitzpatrick [9], [10] were the first to use HTS cables instead of copper cables on board of a naval vessel. They inserted HTS power cables into a flexible cryostat, cooled by gaseous helium. According to them, the main advantage of using HTS system is reduction of cost and weight of the system. Using *Re*BCO cables instead of copper cables will also reduce the power consumption significantly [8], [11].

The power reduction that can be achieved mainly depends on the degaussing currents that are needed, since these determine the cryogenic heat load and thus the power requirements. To estimate values for the degaussing currents, both analytical and finite-element models can be used. Analytical models are only available for highly symmetric shapes like spheres and ellipsoids, but they allow for the straightforward evaluation of the influence of geometrical and material parameters. These models can be used to get a first approximation of the current and power requirement of differently-sized degaussing systems, which can then later be refined with numerical tools. To validate the various models, a *Re*BCO degaussing demonstrator was build and tested at the University of Twente. This demonstrator consists of a steel tube surrounded by three *Re*BCO degaussing coils and three copper degaussing coils. Magnetic field measurements were carried out around the demonstrator tube and compared to the COMSOL models.

## II. ANALYTICAL MODEL

The magnetic field around a spherical ferromagnetic shell in a constant background field can be described using a series of equations as described by Baker and Brown [12]. The magnetic field around a spherical shell with current bands outside or inside the shell can be described by solving the Laplace equation for the vector potential A [12]. Because of the superposition principle, the solution for a spherical shell with a constant background field and the solution for a spherical shell with a current band inside or outside of it can be combined into a new solution. The magnetic field around a spherical shell with multiple current bands can also be found using superposition of the individual solutions.
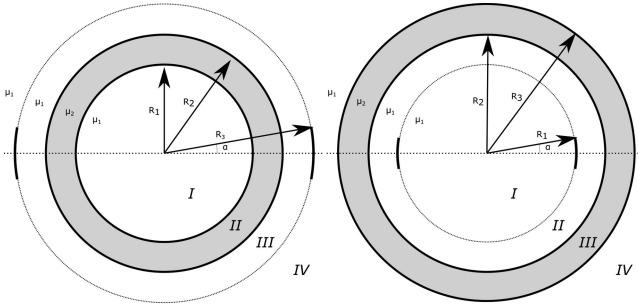
Fig. 1. The variables used in calculating the magnetic field around a hollow sphere with a current band outside or inside of it are illustrated. On the left, the current band is placed outside of the sphere. On the right, the current band is placed on the inside.

All the variables that are used are illustrated in Fig. 1. The left side of the figure schematically shows a spherical shell with a current band outside of it, with the current going inside the page. Region I is inside of the sphere, region II is the spherical shell region III is between the sphere and the current band and region IV is outside of the current band. $R_1$ - $R_3$ and $\mu_1$ - $\mu_2$ describe the different regions while $\alpha$ describes the angle or width of the current band. The same variables are used on the right side of the figure for a spherical shell with a current band on the inside. Solving the Laplace equation of the vector potential A gives a general solution of the form.

$$A = \sum_{n=1}^{\infty} \left[ A_p r^p + \frac{B_p}{r^{p+1}} \right] P_p^1 \left( \cos \left( \theta \right) \right), \tag{1}$$

The coefficients can be found by applying the boundary conditions that both components of the magnetic field should be continuous at $r = R_1$, $r = R_2$ and $r = R_3$. The magnetic vector potential A around the ferromagnetic sphere with a current band around it can then be described using the following equations:

$$A_I = \sum_{n=1}^{\infty} \left[ A_{p1} r^p \right] P_p^1 \left( \cos \left( \theta \right) \right), \tag{2}$$

$$A_{II} = \sum_{n=1}^{\infty} \left[ A_{p2} r^p + \frac{B_{p2}}{r_{p+1}} \right] P_p^1 \left( \cos \left( \theta \right) \right), \tag{3}$$

$$A_{III} = \sum_{n=1}^{\infty} \left[ A_{p3} r^p + \frac{B_{p3}}{r_{p+1}} \right] P_p^1 \left( \cos \left( \theta \right) \right), \tag{4}$$

$$A_{IV} = \sum_{n=1}^{\infty} \left[ \frac{B_{p4}}{r_{p+1}} \right] P_p^1 \left( \cos \left( \theta \right) \right). \tag{5}$$

The coefficients $A_{p1}$, $A_{p2}$, $A_{p3}$, $B_{p2}$ and $B_{p4}$ can be expressed in terms of $B_{p3}$, X, Z, $J'_p(\theta)$ and $J''_p(\theta)$:

$$A_{p1} = A_{p2} + B_{p2} R_1^{-(2p+1)}, \tag{6}$$

$$A_{p2} = X B_{p2}, \tag{7}$$

$$A_{p3} = J'_p \left( \theta \right), \tag{8}$$

$$B_{p2} = B_{p3} Z + J''_p \left( \theta \right), \tag{9}$$

$$B_{p4} = A_{p3} R_3^{2p+1} + B_{p3}. \tag{10}$$

The coefficients $B_{p3}$, X, Z, $J'_p(\theta)$ and $J''_p(\theta)$ are given by (11) shown at the bottom of the next page.

$$X = \frac{-R_1^{-(2p+1)} \left[ 1 + \frac{p}{p+1} \frac{\mu_1}{\mu_2} \right]}{1 - \frac{\mu_1}{\mu_2}}, \tag{12}$$

$$Z = \frac{R_2^{-(p+1)}}{X R_2^p + R_2^{-(p+1)}}, \tag{13}$$

$$J'_p \left( \theta \right) = \frac{\mu_1 J_p \left( \theta \right)}{P_p^1 \left( \cos \left( \theta \right) \right) R_3^{p-1} \left( 2p+1 \right)}, \tag{14}$$

$$J''_p \left( \theta \right) = \frac{J'_p \left( \theta \right) R_2^p}{X R_2^p + R_2^{-(p+1)}}, \tag{15}$$

The variables used are the inner radius of the ferromagnetic sphere $R_1$, the outer radius of the sphere $R_2$, the radius of the current band $R_3$, the relative permeability of the ferromagnetic material $\mu_2$, the relative permeability of the space around the sphere $\mu_1$ and the current distribution $J_p(\theta)$. The current $J_p(\theta)$ can be expressed as a series expansion using associated Legendre functions of the first kind:

$$J_p \left( \theta \right) = \sum_{p=1}^{\infty} J K_p P_p^1 \left( \cos \left( \theta \right) \right), \tag{16}$$

where $K_p$ is given as

$$K_p = \frac{2p+1}{p \left( p+1 \right)} \int_{\frac{\pi}{2}-a}^{\frac{\pi}{2}} P_p^1 \left( \cos \left( \theta \right) \right) \sin \left( \theta \right) d\theta. \tag{17}$$

In a similar way, the magnetic field of a spherical shell with a current band on the inside of the band can be determined as illustrated in Fig. 1. This field is still described by equations 1, 2, 3 and 4, but the coefficients change. Also the magnetic field around a ellipsoid with or without current band can be determined.

## III. FINITE ELEMENT MODEL

In addition to the analytical model, a COMSOL model was created to model the magnetic signature of several objects. Initially, spheres and ellipsoids with and without current bands were modelled to compare the COMSOL model to the analytical models. Finally, also a cylindrical shape was modelled to compare the COMSOL model to the measurements that were carried out as described in the next section.

## IV. MAGNETIC MEASUREMENTS

Magnetic field measurements were performed around a demonstrator tube, shown in Fig. 2. A rail is placed on the ground on which the cart shown in Fig. 3 is placed. A fluxgate magnetometer is placed on the cart which registers the magnetic field in three directions as a function of the distance travelled. Both the measurement rail and the cart consist solely of nonmagnetic materials like aluminum, plastic and brass. The magnetic field is measured at several different heights, ranging from 400 mm to 600 mm beneath the demonstrator tube.
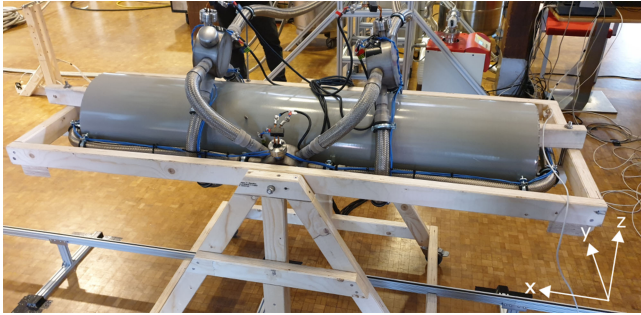
Fig. 2. The demonstrator tube is shown. Two sets of coils, each consisting of 3 coils are placed around the tube. The copper coils (blue cable) consist of 3 windings, while the *Re*BCO coils (inside the stainless steel cryostat) consist of a single winding.



Fig. 4. The measurement setup is illustrated, the magnetic field is measured at 5 different distances below the central axis of the demonstrator tube, h1-h5.
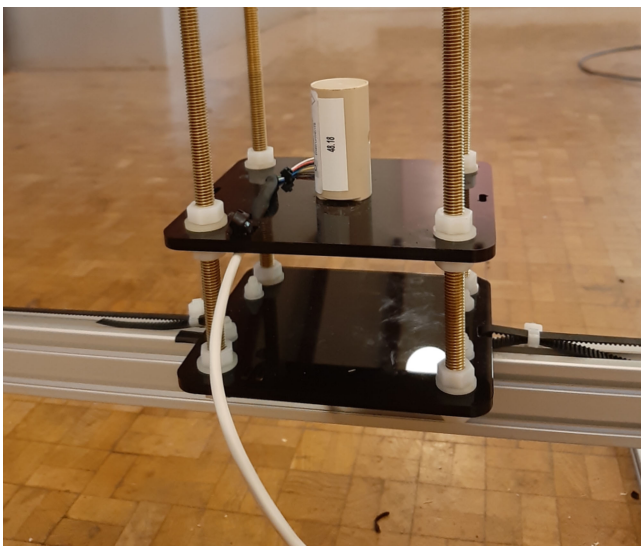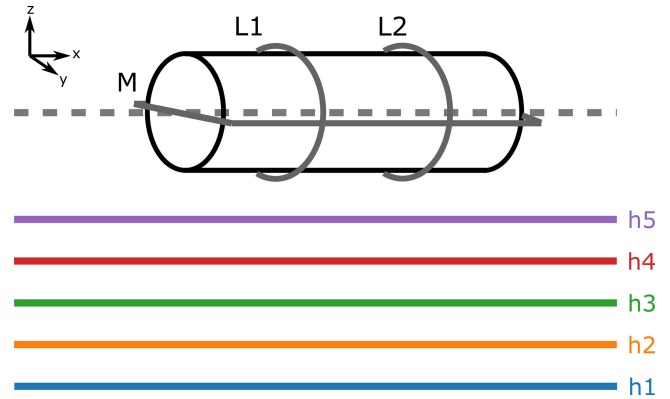


Fig. 3. The cart moving over the measurement rail. A magnetometer is placed on top of the cart, of which the height can be varied.

In Fig. 2, the different degaussing coils that were placed around the demonstrator tube can be seen. In total, 6 coils were used, which can be divided into three pairs consisting of one copper coil and one *Re*BCO coil. The first pair is placed around the length of the demonstrator tube therefore creating a magnetic field in the z-direction, these are called the Main coils (M-coils). The second pair of coils is placed around the circumference of the demonstrator tube, 300 mm away from the middle of the tube, these are called the Longitudinal coils (L-coils). The third pair of coils is also placed around the circumference of the tube, but on the opposite side. The L1 and L2 coils thus create a field in the x-direction. The coil locations and measurement heights are illustrated in Fig. 4.

First, measurements were performed to determine the background field at the measurement location. The background field was determined to be $-18.2 \ \mu T$ in the positive x-direction and $-42.2 \ \mu T$ in the positive z-direction, the field in the y-direction was negligible, far below a $\mu T$.

A second set consists of measurements with the demonstrator tube present. The magnetic field beneath the demonstrator tube is measured at several heights. By subtracting the background field (as a function of height) from this measurement the contribution from the steel tube to the magnetic field can be found. To make sure that the measurements are reproducible, the demonstrator tube was demagnetized as well as possible before the experiments. This was achieved by placing several additional coils in different directions around the demonstrator and creating a slowly reducing alternating magnetic field.

For a third set of measurements, the magnetic field was measured while the current in the different copper and *Re*BCO coils was varied from 0 to 15 A. All the dimensions of the demonstrator set-up are summarized in Table I.

## V. RESULTS

The results from the analytical model were first compared to the results from the COMSOL model. These match well as can be seen in Fig. 5. Fig. 5 shows the magnetic field around a hollow sphere with dimensions similar to those given in Table I, around the shell a current band is placed with a current of 1 A. There is a background field of 50 $\mu T$. The analytical model and COMSOL model overlap well. A small discontinuity can be seen in the analytical model at 0 m. This is because a limit was used to prevent problems with dividing by zero.

Fig. 6 shows the optimum degaussing current as a function of the diameter of a spherical shell, this is done for a current band on the inside of the sphere. This way the optimal degaussing current, and with this the power requirements for a full-size ship can be

$$B_{p3} = \frac{-\frac{1}{\mu_2} J_p''(\theta) \left[ X(p+1) R_2^{p-1} - (p) R_2^{-p-2} \right] + \frac{1}{\mu_1} J_p'(\theta)(p+1) R_2^{p-1}}{\frac{1}{\mu_1}(p) R_2^{-p-2} + \frac{1}{\mu_2} ZX(p+1) R_2^{p-1} - \frac{1}{\mu_2} Z(p) R_2^{-p-2}}, \tag{11}$$

TABLE I
DEMONSTRATOR PARAMETERS

| Parameter | Value | Unit |
|---|---|---|
| Length | 1.51 | m |
| Outer diameter | 0.32 | m |
| Wall thickness | 5 | mm |
| $\mu_R$ | 270 | - |
| Background field ($B_x$) | -18.2 | µT |
| Background field ($B_y$) | 0 | µT |
| Background field ($B_z$) | -42.2 | µT |
| Measuring length | 4 | m |
| Measurement height (h1) | -600 | mm |
| Measurement height (h2) | -550 | mm |
| Measurement height (h3) | -500 | mm |
| Measurement height (h4) | -450 | mm |
| Measurement height (h5) | -400 | mm |



Fig. 7. The magnetic signature in terms of total magnetic field is plotted as a function of the distance travelled under the tube. The dashed lines show the measured data, the solid lines show the finite element model predictions. The measurements were carried out from 600 mm (h1) to 400 mm (h5) beneath the center of the tube.
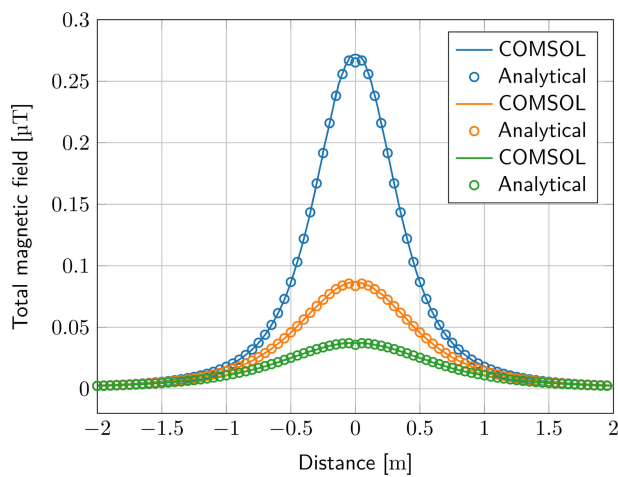


Fig. 5. The analytical and COMSOL model results are compared for calculating the magnetic field around a spherical shell with a current band outside of it. The solid lines show the result of the COMSOL model while the markers show the result of the analytical model. Different colors are used for varying measurement heights, namely 0.5 (blue line), 0.75 (orange line) and 1m (green line) from the center of the sphere.
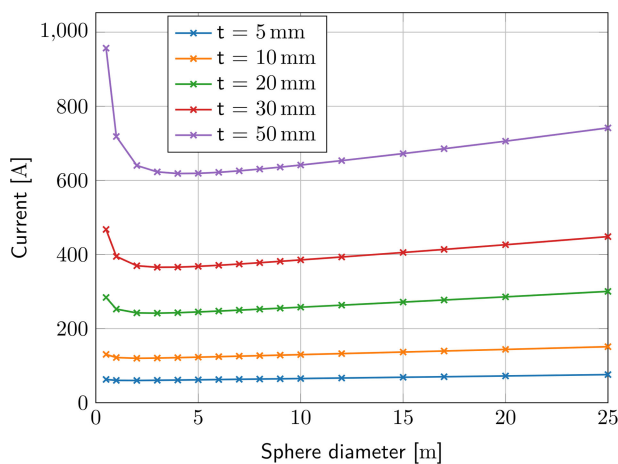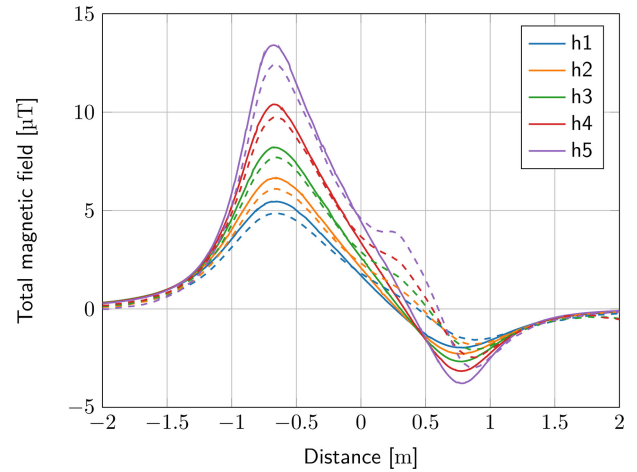


Fig. 6. The analytical solution is used to plot the optimum degaussing current as a function of the size of the object with a relative permeability of $\mu_R = 100$, for several different wall thicknesses.

determined. For each sphere size, the optimal degaussing current is determined at a distance of 1.5 times the sphere diameter. The model can be used to determine the optimum degaussing current as a function of a number of variables including the number of degaussing coils, placement of degaussing coils, wall thickness, relative permeability and size.

The ellipsoid model is also compared to a cylindrical COMSOL model with the same steel volume and similar dimensions. The dimensions used for the cylinder are shown in Table I, while for the analytical model an ellipsoid with a length of 1.51 m and a maximum diameter of 0.4 m is used, with a wall thickness varying between 0.8 and 3 mm. The estimated optimum degaussing current for the ellipsoid when using two longitudinal coils is found to be 16 A, i.e., ∼ 30 % higher than the optimum current of 12 A derived from the cylindrical COMSOL model.

For the experiments the relative magnetic permeability of the demonstrator tube was measured using a VSM. The relative magnetic permeability found to be 270 and is used as an input for the COMSOL model. The magnitude of the magnetic field measured around the demonstrator tube is plotted in Fig. 7, together with the COMSOL model result. Except for the bump that is clearly visible between 0 and 0.5 m in the magnetic field measurement, the measured result matches the COMSOL model very well. The bump that can be seen in is probably due to remnant magnetization in the end plate of the demonstrator tube.

The degaussing coils were used to try and minimize the visible magnetic signature of the demonstrator tube. Since only three coils in two directions were used, the results was not optimal. The result of using a current of 10 A in the M-coil, a current of 12 A in the L1-coil and a current of 10 A in the L2-coil, is shown in Fig. 8. In this case the measurement height is -600 mm (h1). The dashed lines indicate the measurement result, while the solid lines indicated the COMSOL result. The deviation between model and measurement of the signature is quite small, but as soon as the degaussing coils are turned on the
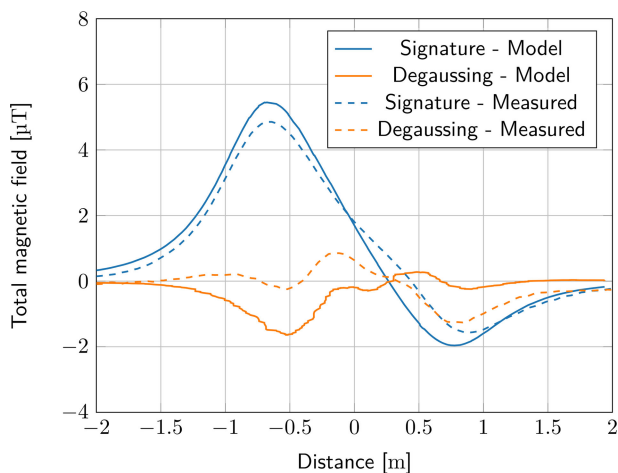
Fig. 8. The total magnetic field is plotted with and without the degaussing coils turned on. The result is not optimal since only three degaussing coils were used. The measurement results and model predictions are shown.

deviation increases. The lines do have the same peaks and dips, yet there is a deviation as large as 1.8 $\mu$T. The reason for this relatively large deviation is unclear and will subject of further study.

## VI. Conclusion

A combination of an analytical model, a finite-element model and magnetic field measurements are used to analyze and optimize a *Re*BCO degaussing system of a tube-shaped demonstrator.

The two different models and measurement results were compared to validate them. The analytical model is as accurate as the finite-element model for simple geometries such as spheres and ellipsoids. Because of its ease of use it can be a powerful tool in evaluating the effect of different parameters such as wall thickness, relative magnetic permeability, number of coils and coil configuration on the optimum degaussing current and, proportional to that, the power consumption of a degaussing system.

The ellipsoid model is also compared to a cylindrical COMSOL model with similar dimensions and the same volume of steel, yielding an optimum degaussing current that is about 30 % different from the analytical one

Additionally, the analytical equations make it easy to scale the degaussing system and give order-of-magnitude values for the power consumption of large systems used in frigates and larger ships.

The result of the finite-element model agrees well with the measured magnetic field profiles. When the degaussing coils are switched off, there is only a small deviation between the model results and the measured results. When the degaussing coils are turned on, for not clarified reasons the deviation is somewhat larger. The model was used successfully to validate the analytical model and can thus be used to estimate the power requirements of much larger systems when more accurate values are needed.

## References

[1] J. Holmes, "Exploitation of a ship's magnetic field signatures," 2016.
[2] J. Holmes, "Reduction of a ship's magnetic field signatures," *Morgan Claypool*, 2018.
[3] A. Modi and F. Kazi, "Magnetic-signature prediction for efficient degaussing of naval vessels," *IEEE Trans. Magn.*, vol. 56, no. 9, Sep. 2020, Art. no. 6000606.
[4] R. A. Raveendra Varma, "Design of degaussing system and demonstration of signature reduction on ship model through laboratory experiments," *Phys. Procedia*, vol. 54, pp. 174–179, 2014.
[5] R. A. Thomas, "Magnetic signatures of spherical in earth's magnetic field—A comparison of analytical and finite element analysis solutions," Australian Government, Department of Defence, Technical report DST-Group-TR-3530, 2018.
[6] M. Isa *et al.*, "An overview of ship magnetic signature and silencing technologies," 2019.
[7] G. Li, D. Zhang, Y. Su, Z. Wang, and W. Tang, "Research on optimization of degaussing current of submarine based on improved cuckoo algorithm," in *Proc. Chin. Automat. Congr.*, 2020, pp. 4595–4599.
[8] R. Ross, C. G. Meijer, and R. J. Mheen, "Degaussing by normal and superconductive windings," in *Proc. 11th Int. Nav. Eng. Conf. Exhib.*, 2012.
[9] B. K. Fitzpatrick, E. M. Golda, and J. T. Kephart, "High temperature superconducting degaussing—Cooling two HTS coils with one cryocooler for the littoral combat ship," in *Proc. AIP Conf.*, 2008, vol. 985, pp. 277–283.
[10] J. T. Kephart, B. K. Fitzpatrick, P. Ferrara, M. Pyryt, J. Pienkos, and E. M. Golda, "High temperature superconducting degaussing from feasibility study to fleet adoption," *IEEE Trans. Appl. Supercond.*, vol. 21, no. 3, pp. 2229–2232, Jun. 2011.
[11] I. Hanse, D. Wikkerink, C. Vermeer, H. Holland, M. Dhallé, and M. ter Brake, "Cryogenics for an HTS degaussing system demonstrator," in *Proc. 15th Int. Nav. Eng. Conf. Exhib.*, 2020.
[12] F. Baker and S. H. Brown, "Magnetic induction of spherical and prolate spheroidal bodies with infinitesimally thin current bands having a common axis of symmetry and in uniform inducing field, a summary," *Final Rep. Nav. Ship Res. Develop. Center*, 1982.